Monitoring and Modeling of the Marine Coastal Environment*

Abstract

The need for better monitoring and modeling of the marine environment has increased dramatically in recent years, in particular, along coastal boundaries and shelf regions where human activities are extensive and pollution has a significant impact. This has been documented in a number of unpredicted events along the coast of Norway, such as storm surges, harmful algal blooms, and oil spills. Systematic integration of remote sensing observations, field observations, and numerical model results is critical for such improvement. We will demonstrate this by presenting examples of (1) model validation by spaceborne infrared (IR) and synthetic aperture radar (SAR) remote sensing observations; and (2) water quality monitoring and simulation using airborne spectrometry and models. High resolution, coupled physical-chemical-biological models, as well as implementation of data assimilation schemes, are needed before a dedicated system for monitoring and forecasting of the coastal environment can become fully operational.

Introduction

In recent years the rich marine environment along the coast of Norway has been repeatedly threatened by unpredicted toxic algae blooms and uncontrolled oil spills. For example, during *Chrysochromulina polyepis* bloom in the Skagerrak in the spring of 1988 (Dundas *et al.*, 1989), the fish farming industry along the southern coast of Norway suffered losses on the order of 30 million NOK, while caged salmon from sea farms along the west coast of Norway at a market value of about 1.2 billion NOK were saved by towing the farms northwards into the fresher and colder water in the fjords. Toxic blooms are generally assumed to be dependent on (1) hydrodynamical conditions, (2) the supply of macronutrients to the euphotic zone, (3) surface solar radiation, and (4) the optical properties of the water column. The Norwegian Coastal Current NCC) that flows out of the Skagerrak along the coast of Norway is the major outlet to the North Sea. Pollution or toxic algal blooms originating in the Skagerrak and the North Sea will be spread by advection from the NCC and threaten the marine environmental along the southern and western coasts of Norway.

The complicated coastal topography, including combinations of fjords, trenches, narrow and wide shelves, and steep continental shelf breaks, has a significant impact on the mesoscale circulation pattern of the NCC as well as on the frontal boundary with the water of Atlantic origin. The interaction with fjord circulation is primarily through wind-driven coastal upwelling dynamics and fresh water run-off in the fjord, and depends on the sill depth at the fjord mouth. The hydrographic, velocity, and environmental conditions in the fjord are therefore a mixture of local effects such as river runoff, spill water, and pollution discharge, as well as the effects of advective processes. These factors have a negative impact on the marine environment in some fjords to such an extent that fishing is prohibited.

Hitherto, oil spills along the coast have been relatively minor, but still with significant local damage. Towards the next century there will be increasing offshore activity in the North Sea, which implies growing ship traffic to and from oil and gas terminals. Therefore, the risk of a hazardous oil spill in the fjord and coastal areas will increase. The concern about the marine environment is therefore growing. A major toxic algae bloom, or a large oil spill due to ship collision, grounding, or sinking, can have dramatic ecological consequences and severe socio-economic impact. In particular, marine wildlife populations, including fish, sea birds, and breeding seals, will be threatened. The local fish-farming and coastal fishing industries may suffer severe losses. In addition, increasing recreational activities in the region will be threatened.

Preparations are now underway for the development of a systematic management tool for the operational monitoring and prediction of the spreading of marine pollution for the coastal region of Norway. This will enable early warning and execution of cost effective precautions in the case of an oil spill or toxic algae bloom. In this paper we will provide an overview of the important elements of this management tool. Monitoring and modeling of coastal and fjord conditions is discussed in the next section, in particular, the need for synoptic remote sensing data validation of simulation models, as well as examples of a toxic algae bloom in Skagerrak, and water quality model simulations in the Oslofjord. Examples, of the preliminary application of data assimilation techniques are provided in the third section, followed by a summary and recommendations.

Monitoring and Modeling

NOAA AVHRR satellite images (Figure 1) clearly show that mesoscale (30 to 100 km) eddies are dominant dynamic features in the NCC (Johannessen and Mork, 1979; Johannessen *et al.*, 1983). The two dominant water masses within the NCC sys-

*Presented at the First Thematic Conference on Remote Sensing for Marine and Coastal Environments, New Orleans, Louisiana, 15–17 June 1992.

Johnny A. Johannessen, Lars P. Røed, Ola M. Johannessen, Geir Evensen, Bruce Hackett, Lasse H. Pettersson, Peter M. Haugan, and **Stein Sandven**
Nansen Environmental and Remote Sensing Center, Edvard Griegsvei 3A, Solneimsvik, Bergen N-5037, Norway.

Robert Shuchman
Environmental Research Institute of Michigan, P.O. Box 134001, Ann Arbor, MI 48113-4001.

Photogrammetric Engineering & Remote Sensing, Vol. 59, No. 3, March 1993, PP. 000–000.

Photogrammetric Engineering & Remote Sensing, Vol. 59, No. 3, March 1993, pp. 351–361.

0099-1112/93/5903–351$03.00/0

tem are fresh coastal water and saline Atlantic water. These waters are distinguished by a temperature contrast of up to 5°C in winter and spring. However, during summer and fall the temperature front gradually vanishes. Ikeda *et al.* (1989) conclude from results of a quasi-geostrophic (QG) two-layer simulation model that baroclinic instability is the primary mechanism for generation of mesoscale eddies along the west coast of Norway, but add that topographic steering makes an important contribution to initial meander generation. These results have been supported by simulation studies using a primitive equation model by James (1991) who concludes that, when the wind field has a minor impact, a QG model provides realistic stream function and circulation estimates of the coastal current.

Monitoring and modeling of the marine coastal environment along the coast of Norway is presently handled by applying the scheme illustrated in Figure 2. Of critical importance is the understanding of the mesoscale circulation pattern, including the behavior of the frontal boundaries as well as the processes responsible for the generation and evolution of mesoscale eddies and upwelling filaments. Infrared (IR) remote sensing of sea surface temperature (SST) distribution enables observations of such features through their temperature contrasts as illustrated in Figure 1. However, the regular use of such images is hampered by the presence of clouds and by weak SST gradients during summer and fall. Synthetic aperture radar (SAR) images available from the European Space Agency (ESA) remote sensing satellite (ERS-1), formed through resonant Bragg scattering of surface waves (developed in response to wind stress), are, on the other hand, weather independent (Wright, 1978; Hasselmann *et al.*, 1985). The spatial distribution of these waves is correlated with a number of significant larger scale processes, including local wind field variations, mesoscale circulation patterns, and internal waves (Johannessen *et al.*, 1991; Lyzenga, 1991). In addition, the presence of pollutant and natural oil slicks at the sea surface can be expressed as dark features in SAR images, through damping of the Bragg waves (Krishen, 1973; Alpers and Huhnerfuss, 1989). Recent ERS-1 SAR images from the NCC clearly document this (Figure 3).

Limited studies have been directed toward the determination of how these mesoscale oceanographic features affect biology, although observations in general suggest that biological distribution in the ocean responds to the presence of fronts, mesoscale meanders, and eddies (LeFevre, 1986; Woods, 1988). In particular, frequent patchiness observed in biological activity, including phytoplankton production as well as observed trapping of egg and fish larvae, are reported to be related to the mesoscale circulation pattern (Rey, 1981; Saetre, pers. com., 1983). However, these relationships are far from completely understood. Similarly, it is anticipated that oil spills can be trapped by mesoscale circulation patterns such as eddies, in particular, during low to moderate wind forcing. Presently we lack a dedicated remote sensing instrument for regular monitoring of primary water quality parameters (Figure 2). This will change with the launch of the NASA SeaWiFS (Sea viewing Wide Field of view Sensor) in 1993, providing multiband visible and near infrared measurements.

IR and SAR images together with radar altimeter and imaging spectrometer sensors form the basis for multisensor remote sensing of the coastal environment. Validation of these kinds of data has been undertaken over several years. However, the availability of synpotic remote sensing observations is presently too limited in time to enable evolution monitoring at characteristic time scales between 1 and 10 days. It is, therefore, necessary to combine remote sensing monitoring with modeling tools, where the models provide high temporal and spatial resolution, are eddy resolving, and are capable of accounting for wind forcing as well as topographic steering. As indicated in Figure 2, we apply relatively simple

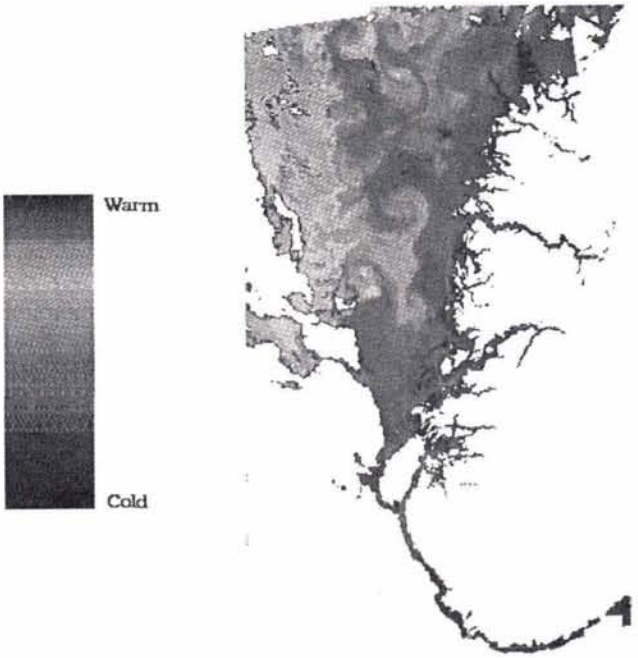

Figure 1. NOAA satellite infrared (IR) image of the meandering Norwegian Coastal Current along the west coast of Norway. Clouds are marked in white. Temperature grey scale range from dark (3°C) in the coastal water to light (7°C) in the Atlantic water.

I. GEOPHYSICAL FEATURES AND PROCESSES	SURFACE REMOTE SENSING MONITORING BY				MODELING BY		
	Visible & Near IR	Thermal IR	SAR	RA	QG	RG	Tracer
TEMPERATURE FRONTS		☼					
CURRENT FRONTS	☼		☼	☼	✔	✔	
MESOSCALE EDDIES	☼	☼		☼	✔	✔	
UPWELLING FILAMENTS	☼	☼	☼		✔	✔	
WIND FRONTS			☼	☼			
II. WATER QUALITY							
ALGAE BLOOMING AND SPREADING	☼						✔[1]
SURFACTANTS	☼		☼				✔
OIL SPILLS	☼	☼	☼				✔
TURBIDITY/SEDIMENTS	☼						✔

☼: Cloud and daylight dependent. ☼: Cloud and daylight independent.

[1] In combination with biological algae modeling.

Figure 2. Overview of important elements for monitoring and modeling of the marine coastal environment. Explanation of the acronyms are Infrared (IR), synthetic aperture radar (SAR), radar altimeter (RA), quasi-geostrophic (QG), and reduced gravity (RG).

quasi-geostrophic (QG) multilayer and reduced gravity (RG) models for this purpose. A major component missing in Figure 2 is the coupling between bio-chemical models and physical models. A crude way around this has been to implement passive advection-diffusion models, based on output from the circulation models, for simulation of drift pattern and eventual sedimentation of algae, oil, or other pollutant material. Experiences from application of the system shown in Figure 2 for environmental coastal ocean monitoring and modeling along the coast of Norway are further presented by some examples below.

Validation of Geophysical Model Results by Remote Sensing Observations.

The two-layer QG model mentioned above has been implemented for the west coast of Norway. Horizontal lengths of about 5 km are resolved. Basic equations in the model express the conservation of potential vorticity in an inviscid flow over gentle bathymetry on an f-plane (Ikeda and Apel, 1981). The initial flow pattern (stream function) in the upper layer was chosen to represent the observed surface temperature distribution of a satellite IR image, in particular, accounting for the large meander over the topographic ridge upstream. This is a crude way of accounting for frontal boundaries in a model which cannot simulate outcropping isopycnals. Maximum current speed of the jet, $u = 0.30$ m/s, was obtained from direct current measurements.

As concluded by Ikeda *et al.* (1989), baroclinic and barotropic instability and interactions with some major topographic features are shown to be capable of producing meanders and detached eddies like those observed in the *in situ* and remote sensing data set (Figure 4). Coast-fjord exchange and local wind effects are not taken into account in these model simulation studies. For the time period considered, winds were generally low and not expected to influence the mesoscale circulation significantly. For more general situations, local wind should be included.

Synoptic observations of the mesoscale circulation in the Norwegian Coastal Current off the west coast of Norway are used to test and improve these model predictions. First, the dense sampling of ship-mounted Acoustic Doppler Current Profiler (ADCP) data collected during an eddy tracking experiments (Johannessen *et al.*, 1989) has been interpolated using an objective analysis (OA) technique (Bretherton *et al.*, 1976;

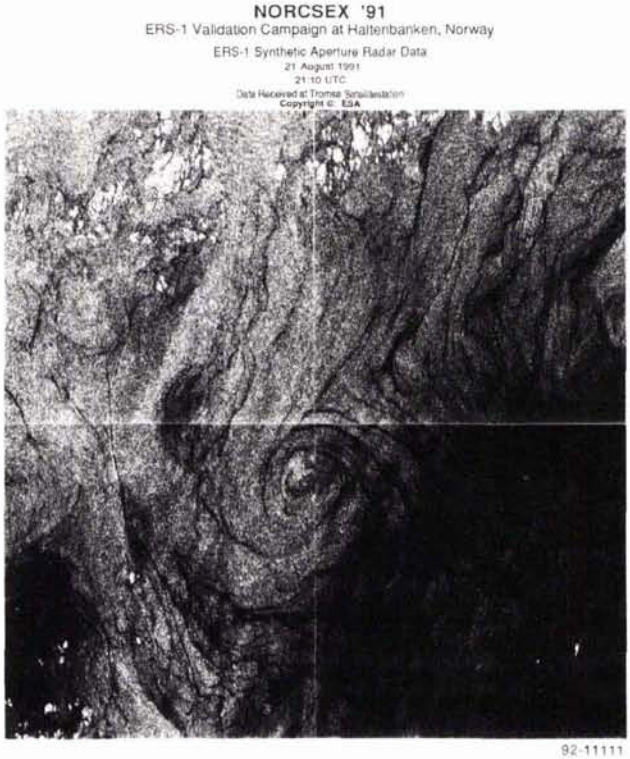

Figure 3. SAR image of the cyclonic eddy in Frohavet received at Tromso Satellite Station at 21 10 UTC on 21 August 1991. The image is a blowup of a standard scene (100 km by 100 km) with a size of 25 km by 25 km. The pixel size is 100 m and represents the local average in a full resolution image. The bright point return in far range is caused by a ship, whereas larger bright returns in near range and along the image top are coastal islands. Data reception and SAR processing were carried out at Tromsø Satellite Station. The image was processed at the Nansen Environmental and Remote Sensing Center.

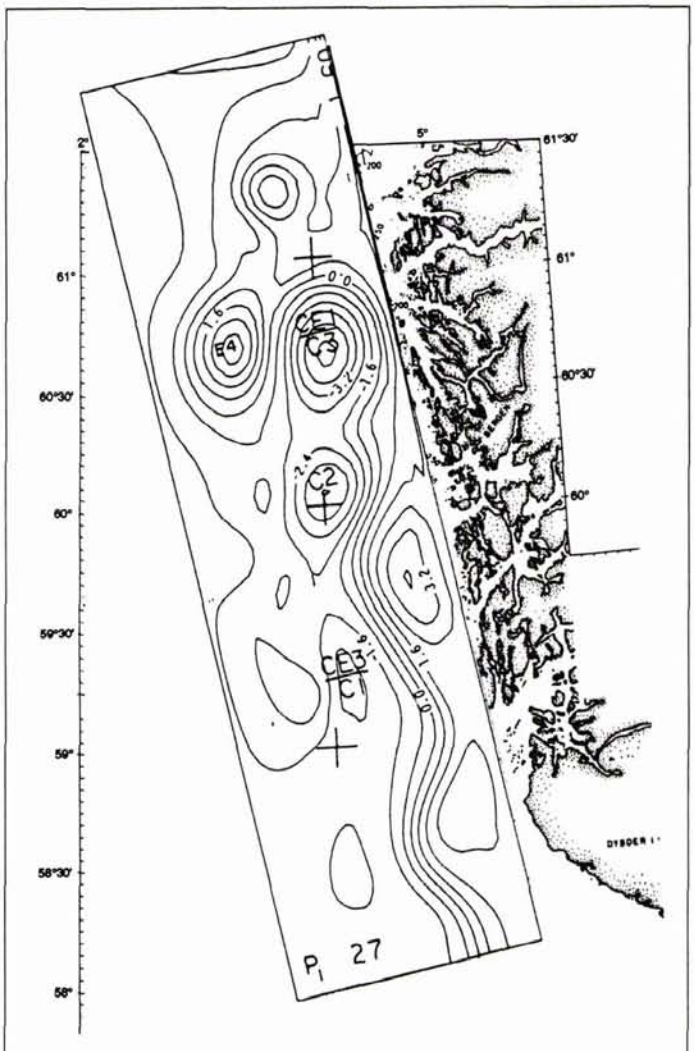

Figure 4. Streamfunction in the upper layer showing formation of eddies along the coast. Model domain is 114 km in the offshore and 430 km in the along-shore direction relative to the coast of Norway.

McWilliams *et al.*, 1986; Carter and Robinson, 1987). This objective analysis method, with divergence-free correlation functions (Freeland and Gould, 1976), determines the spatial and temporal correlation structure of the data. The correlation length scale in this case is estimated to about 50 km. Variability in the tidal frequency range is filtered out by using a correlation e-folding time scale of 2.5 days. To avoid complications due to correlated sub-grid scale noise (Clancy, 1983), the available data points are subsampled to 6 to 7 km minimum distance before analysis is performed. The objective analysis procedure also gives an estimate of the errors, assuming perfect statistics. It is emphasized that the actual expected error will be higher than this level, because the assumed statistics in the procedure are not perfect. The error estimate, however, provides a consistent way of discarding estimates in points where the error is likely to be high. The corresponding velocity field (Figure 5a) has theoretical error estimates of less than 2 cm/s and is suitable for temporal and spatial comparison with IR images as well as QG model results (Haugan *et al.*, 1989; Haugan *et al.*, 1991). A sequence of cloud-free NOAA satellite IR images (Figure 5b) is found to be correlated with these velocity data, demonstrating that they can be used for initialization of eddy-resolving models (Johannessen *et al.*, 1989; Ikeda *et al.*, 1989).

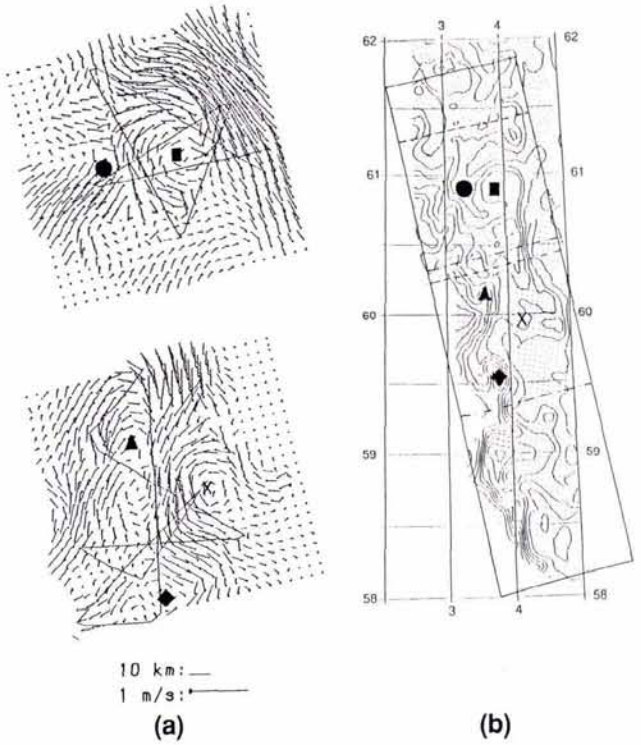

Figure 5.(a) OA velocity maps from ADCP data (ship tracks shown) at 25-m depth obtained from 26 February to 1 March. 5-km grid spacing. Correlation functions from Freeland and Gould (1976): longitudinal velocity correlation f(r) = (1 + br)exp(−br), where b is chosen as 0.032, i.e., length side is 50 km. Signal to noise ratio is 5. Original data are subsampled to 6-7 km minimum distance to avoid problems with correlated noise (Clancy, 1983). (b) Contoured sea surface temperatures (Contour interval 0.5°C) from IR images on 25 and 27 February. The area north of approximately 60°N was cloudfree on 27 February and is combined with the image from the 25 February south of 60°N. Temperature gradient across the frontal zone is 0.2°C/km. Significant features are identified for comparison.

Sensitivity studies are then performed to identify which types of data are most important for precise model forecasts using the simple QG two layer model. Varying initial conditions in the southern part of the model domain have little influence on the evolution in the northern part over a two-week period. However, the baroclinic structure of perturbations is important for the evolution locally. Recirculation of Atlantic water along the western slope of the Norwegian Trench and topographic steering of Atlantic and coastal water contributes to this mesoscale flow pattern. The model is very sensitive to the vertical structure, indicating that initialization and prediction would improve if IR images were supplemented by subsurface data.

Recent validation of upper layer current simulation results by the first ESA ERS-1 SAR data has also been carried out. The eddy depicted in the SAR image (Figure 3) is located in the southern region of Frohavet on the west coast of Norway. The image manifests the existence of an eddy by the dark backscattering lines outlining a cyclonic spiral with an approximate diameter of 5 km. We lack a sequence of SAR images; hence, the temporal characteristics of this eddy, i.e., whether it is forming, fully developed, or decaying, cannot be determined. Light winds varying from 2 to 5 m/s were reported during the SAR overpass, but no surface data are available to offer sufficient analysis of the physical (and biochemical) conditions within the eddy. Despite this, the assumption is that the delicate balance between the wind field, surface current pattern, and concentration of surface slicks is expressed as the spiraling lines of low backscatter embedded in the larger scale orbital motion of an eddy in the upper ocean. The spiral suggests convergence towards the eddy center. Similar converging spiral structures have been observed in aircraft photography and shore-based radar images of ice edge eddies (Johannessen *et al.*, 1987). Such eddies may indeed cause a spiraling path of any pollutant material. In clear weather the High Resolution Visible (HRV) instrument operated on the SPOT satellite can detect such eddy features through the sun glitter induced by the surface slicks. Unless the dark spiral lines also are characterized by a distinct temperature change of more than 0.5°C, no other presently available remote sensing technique will detect the surface expression of an eddy with a 5-km diameter. Such observations are clearly of importance for studies of mesoscale coastal circulation. Moreover, they offer an excellent opportunity for comparison with and validation of model simulations of surface current patterns. This has been done with a reduced gravity model and it is further described below.

In the model formulation, the ocean is assumed to consist of two incompressible, hydrostatic, homogeneous layers of different densities, and the upper layer reference thickness is assumed to be small compared to total water depth. The effect is to eliminate the barotropic mode, so that the response of the model consists of one single baroclinic (internal) mode only. For details concerning the model equations and other considerations, the reader is referred to Luther and O'Brien (1985) and Hackett *et al.*, (1992). The model calculates upper layer currents and densities, and is forced by the observed winds. Open boundaries and rivers are handled by a Flow Relaxation Scheme (FRS) (Martinsen and Engedahl, 1987). The grid size of the RG model was 1.8 km, in comparison to the typical internal Rossby radius of deformation for the region of approximately 7.5 km. Along solid boundaries, the normal no-slip condition applies. The model response

displayed in Figure 6 is taken after a southerly wind event south of Frohavet. The wind field condition prior to SAR data acquisition indeed favors propagation of a downwelling Kelvin wave northeastwards along the coast. With an internal propagation speed of about 1 m/s (the average model phase speed), it will reach Frohavet within 54 hours, in agreement with SAR data acquisition time. Because the Kelvin wave propagates with the coast to the right (northern hemisphere), it will turn southward along the plateau as it enters Frohavet. Positive vorticity is then created within Frohavet as the wave turns at the head and leaves along the eastern boundary. The model dynamics, in turn, allow barotropic instability to grow and to form a cyclonic eddy (Figure 6), in good agreement with the SAR observed eddy (Figure 3). The cyclonic orbital motion in the eddy is about 0.20 m/s. In correspondence with this, the interface height domes upwards about 10 m towards the eddy center. The convergence towards the eddy center, qualitatively indicated in the SAR image, cannot be accurately quantified from model outputs in this case due to insufficient spatial resolution in the model.

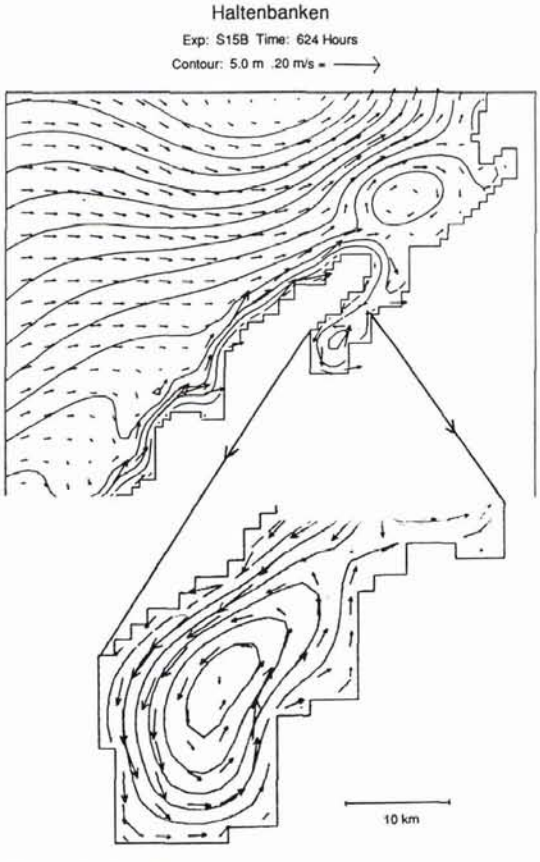

Figure 6. Circulation pattern obtained from RG model after two months of simulation. Land contours are chosen to correspond approximately to the 20-m isobath, which causes Forhavet to be displayed as a fjord running southwest to northwest with its open end towards the north. Arrows mark flow direction and strength. Contour lines indicate departure from initial upper layer thickness of 50 m at 5-m intervals. Maximum departure is found along the coast in association with the presence of the downwelling Kelvin wave. The blowup shows the cyclonic eddy in Frohavet for comparison to Figure 3.

The combination of model results and SAR observations may also provide opportunities for discriminating between natural surface slicks and man-made oil spills. The microlayer of surface slicks is relatively fragile compared to pollutant oil slicks, and the interaction of this layer with the surface current can more systematically reconfigure in line with the larger scale surface current flow. With acces to the surface current pattern from model output, one can thus compare the slick configurations. Pollutant oil spills may be better characterized by high concentration spots with very distinct boundaries to the surroundings. In addition, expressions of such pollutant oil spills are expected to survive longer in strong winds.

A Toxic Algae Bloom along the Coast.

The first documented observation of a toxic algae bloom was reported from the west coast of Sweden on 9 May 1988, while dead fish were first observed on 13 May (Dundas *et al.*, 1989). The bloom along the west coast of Norway culminated in the beginning of June. During the bloom, maximum algal concentrations in the surface layer (upper 30 m) were measured up to a maximum of 90 million algal cells per litre of water. Early during the bloom, observations indicated a close correlation between the spreading and advection of the algae and the drift of warm surface monitored by a sequence of satellite IR data obtained during cloud-free periods. Between 15 May and 30 May a drift ranging from 5 to 30 km/day was estimated, in agreement with typical reported currents (Figure 7). Expected evidence of meanders and eddies with scales of 30 to 60 km were also observed in the NCC as the process of advection pushed it northwestward out of the Skagerrak. In particular, a large meander southwest of Stavanger is noticeable on 22 May overlying a topographic ridge, in agreement with topographic steering suggested by Ikeda *et al.* (1989).

In order to forecast the algal drift up the coast of western Norway, and simultaneously provide a sampling scheme for the direct measurements, the two-layer QG model was applied in combination with the IR images (Johannessen *et al.*, 1989). Necessary estimates of layer thickness and current speed were taken from climatological data and direct observations. The algal drift was estimated by the ADCP currents at 14 m and 22 m with a mean northward speed of the NCC of about 0.25 m/s (25 km/day), in general agreement with the advection speed derived from the sequence of satellite IR images. The stream function was kept constant along the two closed boundaries, and radiation conditions were applied at the open downstream (northern) boundary. The wind records indicate minor wind effects during the simulation experiment, implying that the omission of wind effects in the model is valid. Furthermore, outer fjord and coastal exchange processes are omitted in the model.

An initial meander over the ridge upstream, taken from the IR image, is seen to develop into a vortex pair on 28 May with an anticyclonic eddy near shore (Figure 8a). This pair intensifies during the next couple of days but remains nearly stationary. Downstream of the pair, the major current flows towards the coast. Simultaneously, meanders propagate further downstream. As they grow, cyclonic eddies are generated upstream as a result of vortex stretching, conserving potential vorticity. The mutual feedback between the meander and cyclonic eddy develops a backward-breaking meander on the offshore side of the cyclonic eddy. The evolution of the stream function pattern is in good agreement with direct current measurements, in particular, featuring the major

semi-stationary meandering flow upstream, the anticyclonic feature over the topographic ridge, and the presence of a vortex pair with the cyclonic eddy near the coast in the model interior. The results are also in good qualitative agreement with the sequence of high quality IR images.

On the assumption that algae drift passively with the current and that local blooms are minor, the advection of a simulated algal front was also investigated in a tracer model from 26 May to 1 June (Figure 8b). The initial position represents the observed position of the algal front on 26 June. The downstream evolution of the trajectories shows a meander-like propagation pattern, in agreement with the vortex pair displayed by the stream functions. The central part of the front propagates downstream at an average speed of 20 to 25 km/day. The particles placed nearshore first follow a counterrotating anticylonic path, but continue northward near the coast instead of turning southward. In contrast, the particles on the offshore edge of the jet-like current follow cyclonically curved trajectories in accordance with the formation of the cyclonic eddy offshore. The particles appear to remain trapped in the cyclonic feature. The positions and configurations of the algal front on 30 May and the detached algal plume on 31 May are in good agreement with the results of these tracer simulations. This clearly demonstrates the impact that meander and eddy features may have on the dispersion of biological material. In turn, concentrations of biological material in the eddies can increase.

When wind effects are minor, it once again appears that the QG model simulations may be initiated and evaluated by the surface flow pattern derived from sequences of cloud-free satellite IR images. However, in this case, the lack of systematic monitoring and coupled physical biological modeling prior to the bloom caused the damages and losses to be high. In particular, the absence of any remote sensing sensor capable of directly observing the surface layer distribution of algae biomass was recognized. Such data could have provided early warning as well as important guidance to the *in situ* field observations of the daily evolution of the algal front. This is illustrated by the comparison between chlorophyll-*a* distribution across the Skagerrak obtained on 18 May 1989 with a Compact Airborne Spectrometer Imager (CASI) (Borstad *et al.*, 1987; Pettersson *et al.*, 1992) and *in situ* sea surface observations on 19 May (Figure 9). The CASI spectral data were obtained from a flight altitude of 9,000 feet under relatively good observational conditions. The selection of the spectral data was done as close as possible to the location of

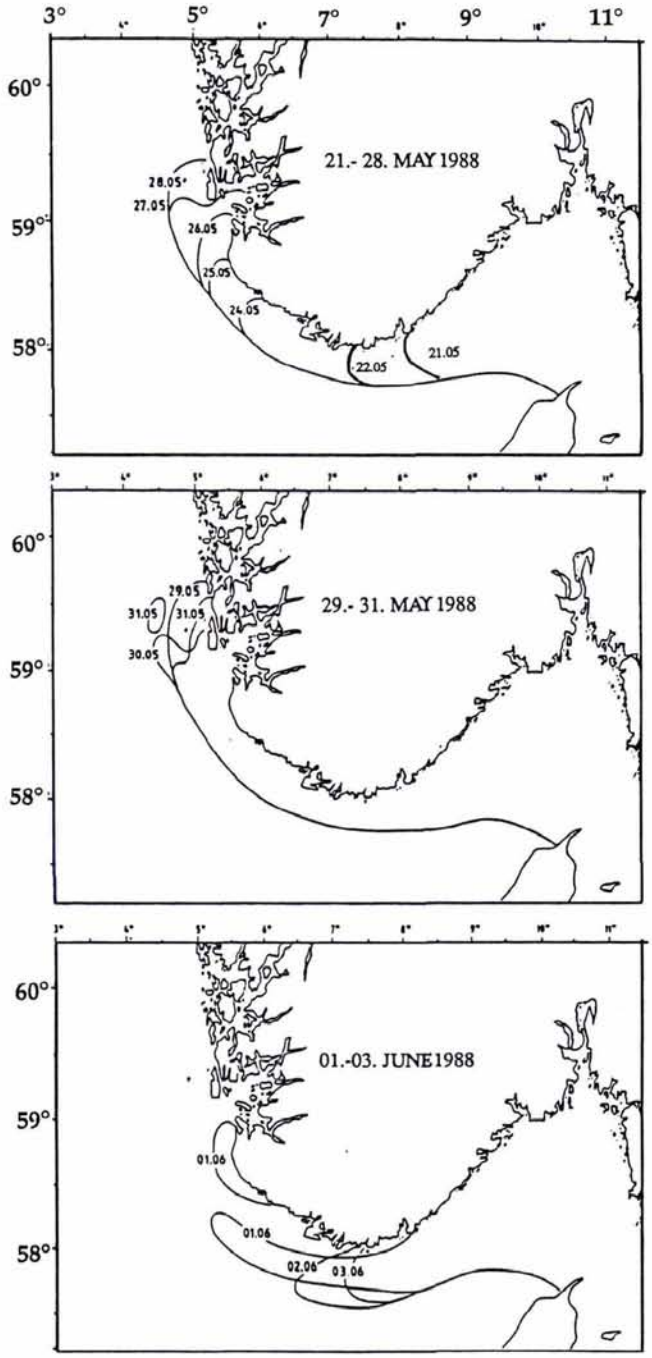

Figure 7. Summary of the observed algal front (including both advance and retreat) in the Norwegian Coastal Current from 21 May to 3 June defined by 0.5 to 1.0 million algal cells per litre. Note that the algal front locations of 21 to 22 May are assumed to be overlapping the temperature fronts inferred from the NOAA satellite IR images.

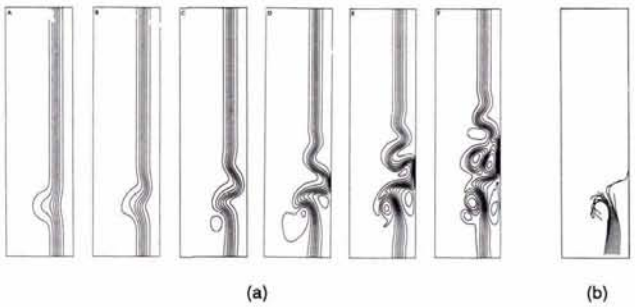

Figure 8.(a) Evolution of the pattern of the streamfunction in the upper layer predicted by the model from 22 May (initial conditions) until 1 June. Further downstream, the growth of new meanders will occur later, but the area remains undisturbed during the simulation period because no local perturbation is initiated and no meanders or eddies (with a typical propagation speed of 20 km/day) can reach that far downstream in only 10 days. (b) Drift trajectories of the algal front as predicted by a passive tracer included in the model simulation on 26 June. The trajectories are drawn based on particle position twice daily.

the ship stations, with additional airborne measurements in-between these ship stations. The along-transect variation of the phytoplankton pigment concentrations, in the surface layer (0 metre), shows generally higher concentrations on the Norweigian side of the basin than along the Danish coast. A minimum Chl-*a* value is observed in the central Skagerrak (station no. 7). Although some station-to-station discrepancies are observed and the overall explained variance is only around 40 percent, there is a larger scale agreement between the FLH and Chl-*a* data with respect to variability across the Skagerrak basin.

Water Quality Simulation in a Fjord.

The effect of eutrophication in the Oslofjord has proven to be an issue of growing concern in what is the most densely populated part of Norway. In order to help elucidate the critical factors contributing to eutrophication, a study of the transport paths in the fjord system was initiated with the objective of explaining the mechanisms and processes which determine the upper layer transport. The system features two major river outflows and has a large opening to the Skagerrak in the south with a sill depth of about 130 m. The relatively simple nonlinear one-active-layer reduced gravity (RG) model is used to simulate and explain the upper layer circulation in the outer Oslofjord during summer. It is forced by the observed winds, the river discharges, and the fluxes on the open boundary to the Skagerrak. The model is implemented with a grid size of approximately 400 by 400 metres. This resolution resolves the complex geometry of the fjord, and is well below the Rossby radius of deformation. The model is, therefore, eddy resolving. As for the toxic algal bloom, the passive transport of pollutants in the upper layer is simulated through a simple tracer model. Sedimentation of particles is handled by a "sink" term whenever the depth of the particles equals the pycnocline depth. The results of some idealized simulation experiments carried out from 1 May through 15 July are considered here (Figure 10). In this period, intensive field programs were carried out, and the collected *in situ* data as well as Landsat remote sensing observations have been used to validate the model results. These results clearly demonstrate that upper layer circulation is dominated by the wind, but that river discharges play an important role. The current pattern is characterized by a number of eddies generated by barotropic instabilities, which significantly affect the fate of passive tracers from the rivers. In general, the model simulation results compare well with observations of currents, density, and water property fields.

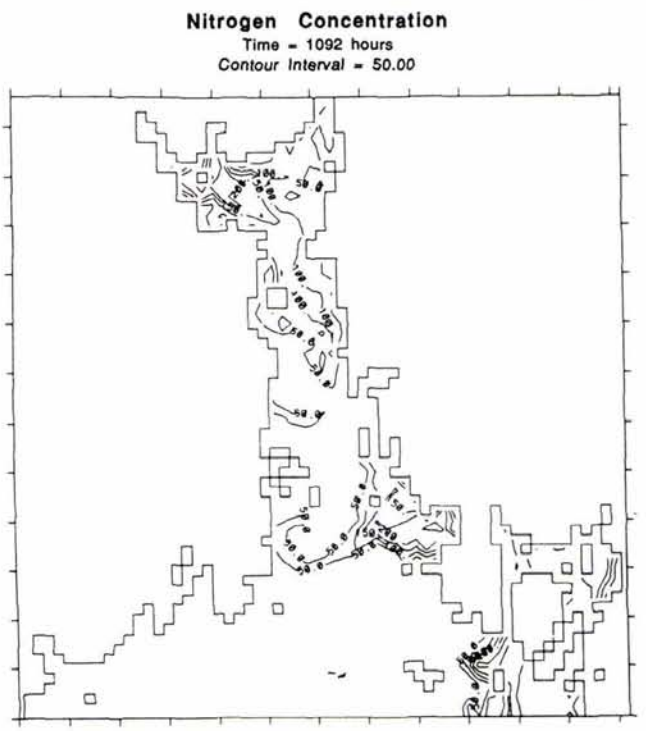

Figure 10. Simulation of particle concentration of nitrogen in the outer Oslofjord.

The model results presented above will never give an exact description of the state of a dynamic system. They will be subject to errors from estimated model parameters, neglected physics, and solution techniques. Nor are the direct measurements ever complete. They are subject to errors, there will always be physics on some scales which are not entirely resolved, and they will only be available sparsely in space and time. Ways to improve that are discussed in the next section.

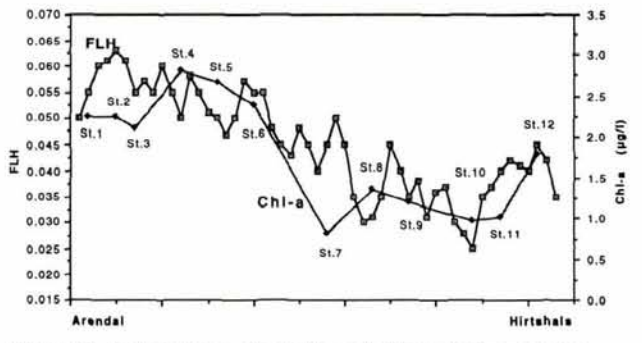

Figure 9. Comparison of profiles of chlorophyll-*a* concentration at the surface across the Skagerrak obtained with the airborne spectrometer technique (FLH) and ship measurements of chlorophyll a concentration.

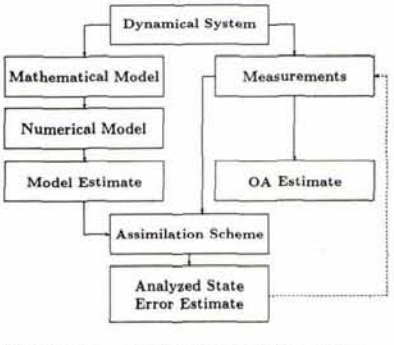

Figure 11. Architecture of the data assimilation scheme, including the dynamical system of simulation models and measurements.

Data Assimilation

A data assimilation system is designed to improve the state estimate by optimal extraction of information from both the measurements and the dynamic model (Figure 11). It may be used to improve initial and boundary conditions, to estimate poorly known model parameters, and to improve error estimates. In turn, it will improve forecasting capability and provide a sophisticated data analysis tool. The measurements are interpolated consistently with the model dynamics, and we get more information out of the data, while the model is constrained by the measurements and will not drift away from the observed state. Furthermore, due to the sampling strategies dictated by the data assimilation scheme (Figure 11), the quality of the database will improve significantly and allow for the discrimination and quantification of various effects required for model improvements. Although data assimilation is well studied in meteorology, in particular in weather forecasting, the sparseness of oceanographic data and lack of ocean circulation and water quality predictions have hampered a similar development for oceanographic models. This is now undergoing changes with the expected increase of oceanographic remote sensing data for the 90s, as well as requirements for monitoring and forecasting of the marine environment. An excellent review of data assimilation methods in meteorology and oceanography is given by Ghil and Melanotte-Rizzoli (1991).

There are two main concepts which have been discussed for data assimilation: the variational/adjoint method and the sequential method. The adjoint method has been the most used scheme (Lewis and Derber, 1985; Talagrand and Courtier, 1987; Courtier and Talagrand, 1987; Long and Thacker, 1989; Thacker and Long, 1988). Given a set of measurements within a certain time interval, the initial conditions and unknown parameters which are sought for the model are those resulting in the model trajectory that best fits the measurements in some sense. This can be formulated as a constrained minimization problem where the ocean model operates as a strong constraint on a cost function measuring the distance between the model solution and the measurements in a time interval. Drawbacks of the method are the difficulty with non-linear systems and with model errors (system noise). This may result in misleading conclusions which depart significantly from the measurements, especially if the ocean model is unable to describe important phenomena which are contained in the measurements.

Sequential methods, on the other hand (see Evensen, 1992), update the model solutions in every time step where measurements are available, starting from some best guess initial condition. This group of methods requires an updating scheme which combines the model solution and the measurements to find a better state estimate. At the same time, it will propagate the previous information which has been assimilated forward in time to increase the knowledge of the system. "Better" normally means that the updated estimate is closer to the data than the previous estimate, and at the same time is smooth and physically acceptable. The methods of direct insertion and the Kalman filter represent the two extremes of updating schemes. "Direct insertion" means that the value from a measurement is directly inserted at the grid point corresponding to the location of the measurement. This may, of course, lead to spikes and discontinuities in the model solution. The Kalman filter (see Gelb, 1974) is the other extreme, where the update is based on information about the statistical properties of the errors in both the measurements and the model state, and therefore the error covariance matrices of both the state estimate and the measurements must be known. The Kalman filter gives the optimal linear update in a least-squares sense, based on the known statistics. It also ensures a smooth update determined by the covariance functions describing the correlation of the errors between variables at different grid points. An example of this filter is optimal interpolation (OI) which has been used by meteorologists for operational weather prediction. In OI a constant error covariance matrix is used in the standard Kalman filter equations to update the state vector when measurements are available. It is not propagated forward in time, and this results in major computational savings. This method has recently been discussed in the context of a QG model by Rienecker and Miller (1991) for oceanographic applications.

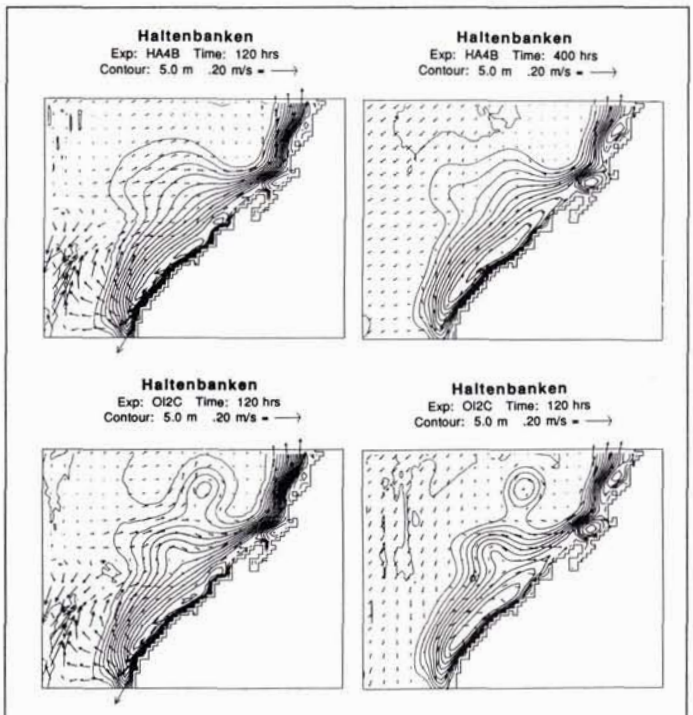

Figure 12. Comparison of simulation results of the circulation pattern with and without the use of Optimal Interpolation (OI).

Optimal Interpolation Experiment.

The RG model of the Norwegian shelf, described in the previous section, and the NORCSEX'88 data set (Johannessen *et al.*, 1991) were used for the purpose of exploring the effect of assimilating real data into an existing ocean model (MOMOP, 1992). While the RG model is relatively simple, it is still a fully nonlinear, eddy-resolving, primitive equation model, implemented with realisitic land boundaries and long open boundaries, and driven by real winds. This necessitated the use of a computationally economic assimilation technique, and OI was chosen. In preliminary simulation experiments, it became clear that the one active layer RG model was inadequate for replicating the variability of the currents and density structures on the shelf, being better in the coastal region. Also, the data assimilated—densities from the current meter moorings—could not resolve the mesoscale. Thus, the assimilation experiment was an effort to assimilate insufficient data into an inadequate model. As such, it is a serious test of the promise of data assimilation. In Figure 12 the model results from data assimilation are compared to the control case with no data assimilated. The assimilated model fields quickly generate anticyclonic eddies about the current meter

sites. This occurs because the observations are biased toward larger upper layer thicknesses in comparison to the model thickness. Hence, regions of deeper upper layers are formed centered around the mooring sites as the assimilation takes effect. In summary, the assimilation exercise, using the OI technique, has shown the following: (1) optimal interpolation is preferable compared to direct insertion because the latter provides no control whatsoever over the error statistics of the model and observations; (2) optimal interpolation is computationally feasible with eddy-resolving models, such as used here; (3) assimilation of data which contain length scales not included in the model simulation results in spurious circulation features such as eddies around data points; and (4) lack of data coverage hinders successful assimilation.

In contrast to OI, the full Kalman filter is extremely expensive to compute, both in regards to number of numerical operations and storage requirement. The propagation of the error covariance matrix requires an amount of computation which is $2n$ times a pure ocean model integration, where n is the number of state variables. Further, the error covariance matrix of size n times n must be stored. The extended Kalman filter (EKF) is an extension of the common Kalman filter and may be used when the model dynamics or the measurement equation is nonlinear. It consists of an approximating equation for the propagation of error covariances, and also approximating filter equations if the measurement equation is nonlinear. The extended Kalman filter has been implemented with the multilayer QG model by Evensen (1992). In oceanography the Kalman filter has been used by Budgell (1986, 1987) to describe nonlinear and linear shallow water wave propagation in branched channels. The Kalman filter has also been used to assimilate wind data in a wind-driven numerical model of the equatorial Pacific (Bennet and Budgell, 1987). With good knowledge of the error statistics, both for the dynamical model and the measurements, the inclusion of error covariance propagation should certainly improve the estimate.

An experiment has been performed to illustrate the difference between the EKF and OI when used with the QG model. A square domain (17 by 17 grid points) with closed boundaries and two layers is used. First, a reference case is generated (left column in Figure 13) where, as initial condition, an anti-cyclonic eddy is standing on a sloping bottom with increasing depth in the y-direction. The eddy propagates along the bottom slope, and behind it a cyclone develops. These two eddies then begin to interact with each other and the boundaries. This somewhat artificial case is used because considerable dynamics are contained in a small do-

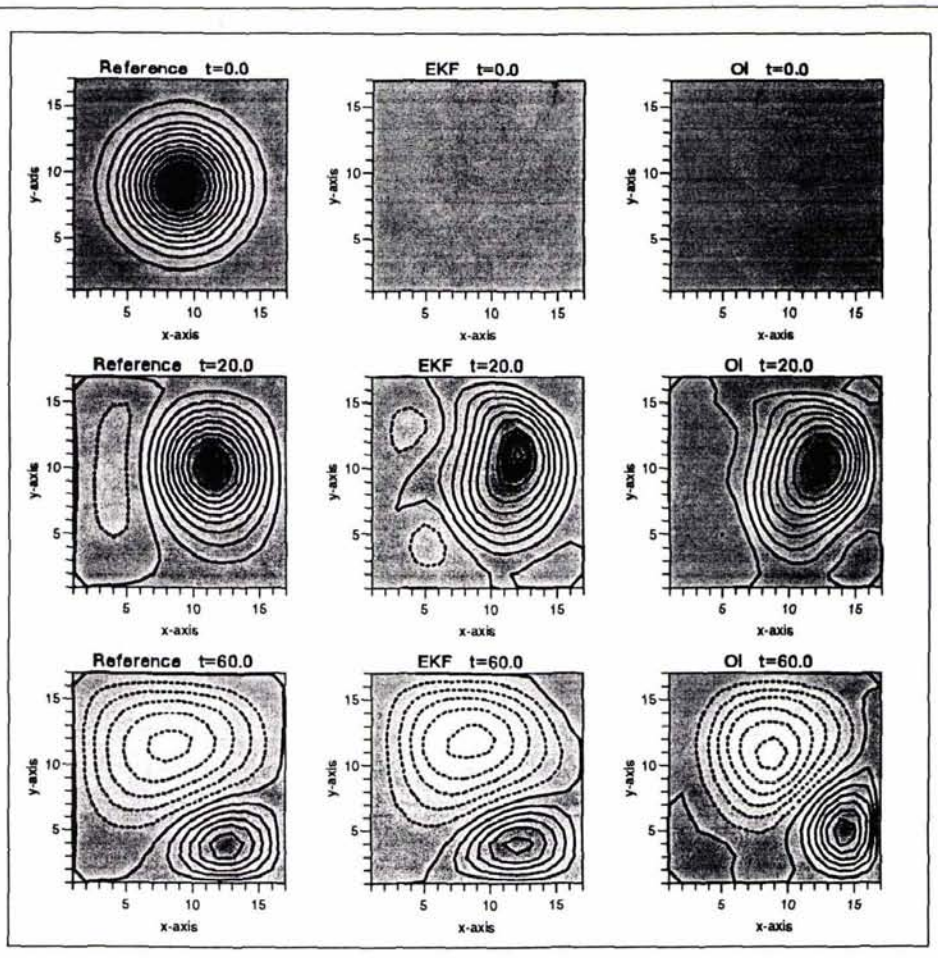

Figure 13. Comparison of data assimilation with use of the extended Kalman filter in contrast to OI methods. The EKF, which includes dynamical propagation of the error covariance matrix, i.e., the error statistics of the state estimate, performs significantly better than the OI method where the error covariance matrix is constant in time.

main. Measurements are generated from the reference solution, by taking stream function values at four locations in the upper layer every $T=2,4,6,...$, ($\Delta t = 0.5$). These measurements are used in the assimilation experiments where the goal is to reconstruct the reference solution with no knowledge about the solution except of the measurements and the model dynamics. In the second and third column of Figure 13, the results from the assimilation experiment are shown. The initial conditions are set equal to zero, but after some time of integration when some of the measurements have been assimilated, the estimates approach the reference solution. The EKF which includes dynamic propagation of the error covariance matrix, i.e., the error statistics of the state estimate, performs significantly better than the OI method where the error covariance matrix is constant in time. Data assimilation using the EKF in realistic ocean circulation models requires super computers with large memory and extremely fast CPUs. Fortunately, such computers are now available which can handle data assimilation using the EKF extended Kalman filter with a QG model for reasonably large grids. The error covariance propagation equation is also very well suited to be computed on the massive parallel computers.

Summary and Recommendation

Today there is no tool for operational monitoring and prediction of spreading of marine pollution available for management of the coastal area of Norway. Therefore, early warning and, hence, cost-effective precautions will be difficult to apply in case of future oil spills, toxic algal blooms, or other pollutant material releases. With this in mind, the Division of Marine Environment and Resources of the Bergen Scientific Foundation with its three marine environmental centers (Institute of Marine Research, Center for Marine Environment; the University of Bergen Centre for Studies of Environment and Resources, including the Geophysical Institute, Division for Oceanography and Meteorology; and Institute for Fisheries and Marine Biology) and the Nansen Environmental and Remote Sensing Center have proposed a 5-year interdisciplinary research and development program to start in 1993. The main goal of the program is to develop an operational marine monitoring and modeling system, including a water quality model for the coastal regions of Norway. The system will be flexible so that it can be adapted to other geographical areas, in particular, around the North Sea and in the Baltic Sea.

In order to reach this goal, an integrated system based on a high resolution atmospheric model and three-dimensional numerical ocean current models coupled to chemical and biological models must be developed. The models will be complemented with dedicated field and remote sensing data, in particular, NOAA IR, ERS-1 SAR, and Sea WiFS multiband imaging radiometer data for data assimilation and monitoring (Figure 14). An operational water quality monitoring and forecasting system based on this concept will provide improved understanding of the marine ecological interplay in fjord and coastal regions, including better knowledge of (1) local and regional surface and subsurface current conditions and variations, with local and regional atmospheric forcing and fresh water supply; (2) the chain of events form meteorological via oceanographic to the biological conditions which leads to the bloom of a toxic algea; (3) the drift pattern and dispersion of any oil spill or toxic algae; and (4) the relationship between the physical environment and biologic systems as well as the driving mechanisms for ecological variability.

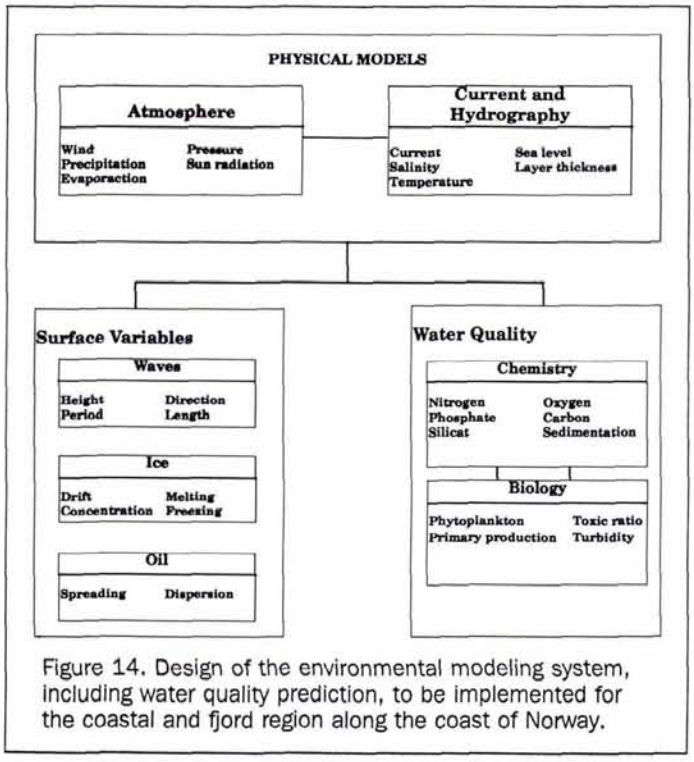

Figure 14. Design of the environmental modeling system, including water quality prediction, to be implemented for the coastal and fjord region along the coast of Norway.

Acknowledgement

The work reported here has been supported by the Norweigian Space Center (NSC), Royal Norwegian Council for Scientific and Industrial Research (NTNF), (NAVF), Operators Committee North (OKN), European Space Agency (ESA), and Office of Naval Research (ONR).

References

Alpers, W., and H. Huhnerfuss, 1989. The Damping of Ocean Waves by Surface Films: A New Look at an Old Problem. *Journal of Geophysical Research*. 94:6251-6266.

Bennett, A.F., and W.P. Budgell, 1987. Ocean data assimilation and the Kalman filter: Spatial regularity. *J. Phys. Oceanogr.*, 17(10):1583-1601.

Borstad, G.A., R.C. Kerr, D.N. Truax, and D. Pan, 1987. *Using an Imaging Spectrometer to Map Phyloplankton Chlorophyll*, Borstad Associates Ltd., for Dept. Fisheries and Oceans, Sidney, B.C., Canada.

Bretherton, F.P., R.E. Davis, and C.B. Fandry, 1976. A technique for objective analysis and design of oceanographic experiments applied to MODE-73. *Deep-Sea Res.* 23:559-582.

Carter, E.F., and A.R. Robinson, 1987. Analysis models for the estimation of oceanic fields. *J. Atm. Oceanic Techn.* 4:49-74.

Clancy, R.M., 1983. The effect of observational error correlations on objective analysis of ocean thermal structure. *Deep Sea Res.* 30(9A):985-1002.

Courtier, P., and O. Talagrand, 1987. Variational assimilation of meteorological observations with the adjoint vorticity equation II: Numerical results. *Quart. J. Roy. Meteor. Soc.*, 113:1329-1347.

Dundas, I., O.M. Johannessen, G. Berge, and B. Heimdal, 1989. Toxic Algal Bloom in Scandinavian Waters, May–June 1988, *Oceanography*, 2:9-14.

Evensen, G., 1992. Using the Extended Kalman Filter with a Multilayer Quasigeostrophic Ocean Model, accepted for publication in *Journal of Geophys. Res.*

Freeland, H.J., and Gould, W.J., 1976. Objectve analysis of mesoscale ocean circulation features. *Deep Sea Res.* 23:915-923.

Gelb, A., 1974. *Applied Optimal Estimation*. MIT Press, Cambridge.

Ghil, M., and P. Malanotte-Rizzoli, 1991. Data assimilation in meteorology and oceanography. *Advances Geophys.* 33:141-266.

Hasselmann, K., R.K. Raney, W. Plant, W.R. Alpers, R.A. Shuchman, D.R. Lyzenga, C.L. Rufenach, M.F. Tucker, 1985. Theory of synthetic aperture radar ocean imaging: A MARSEN view. *Journal of Geophysical Research*. 90:4659-4686.

Hackett, B., L.P. Roed, and T.B. Irmann-Jacobsen, 1992. A model of the winter circulation in the Northwest Approaches to the British Isles forced by observed winds, submitted to *J. Geophys. Res.*.

Haugan, P.M., G. Evensen, J.A. Johannessen, O.M. Johannessen, and L.H. Pettersson, 1991. Modeled and observed mesoscale circulation during the 1988 Norwegian Continental Shelf Experiment. *Journal of Geophysical Research*, 96:10487-10506.

Haugan, P.M., J.A. Johannessen, K. Lygre, S. Sandven, and O.M. Johannessen, 1989. Simulation Experiments of the Evolution of Mesoscale Circulation Features in the Norwegian Coastal Current. *Mesoscale/Synoptic Coherent Structures in Geophysical Turbulence*, pp. 303-313.

Ikeda, M., and Apel, J.R., 1981. Mesoscale eddies detached from spatially growing meanders in an eastward-flowing oceanic jet using a two-layer quasi-geostrophic model. *J. Phys. Oceanogr.*, 11:1638-1661.

Ikeda, M., J.A. Johannessen, K. Lygre, and S. Sandven, 1989. A process study of mesoscale meanders and eddies in the Norwegian Coastal Current, *Journal of Physical Oceanography*, 19:20-35.

James, I.D., 1991. A primitive equation model simulation of eddies in the Norwegian coastal current. *J. Phys. Oceanogr.*, 21:893-902.

Johannessen, J.A., R. Shuchmann, O.M. Johannessen, K.L. Davidson, and D.R. Lyzenga, 1991. Synthetic Aperture Radar Imaging of Upper Ocean Circulation Features and Wind Fronts. *Journal of Geophysical Research*, 96:10411-10422.

Johannessen, J.A., O.M. Johannessen, E. Svendsen, R. Shuchmann, T. Manley, W.J. Campbell, E.G. Josberger, S. Sandven, J.C. Gascard, T. Olaussen, K. Davidson, and J. Van Leer, 1987. Mesoscale Eddies in the Fram Strait Marginal Ice Zone During the 1983 and 1984 Marginal Ice Zone Experiment. *Journal of Geophysical Research*, 92:6754-6772.

Johannessen, J.A., O.M. Johannessen, and P.M. Haugan, 1989. Remote sensing and model simulation study of the Norwegian Coastal current during the algal bloom on May 1988. *Inter. Journ. of Rem. Sens.*, 10(12).

Johannessen, J.A., E.A. Svendsen, S. Sandven, O.M. Johannessen, and K. Lygre, 1989. Three dimensional structure of mesoscale eddies in the Norwegian Coastal current, *Journal of Physical Oceanography*, 19:3-19.

Johannessen, O.M., J.A. Johannessen, and B.A. Farrelly, 1983. Application of remote sensing for studies, mapping and forecasting of eddies on the Norwegian Continental Shelf, *Proceedings of EARSEL/ESA Symposium on Remote Sensing for Environmental Studies*, Brussels, Belgium, 26-29 April. pp. 179-187.

Johannessen, O.M., and M. Mork, 1979. *Remote Sensing Experiments in the Norwegian Coastal Waters*. Report 3/9. Geophysical Institute, University of Bergen, Norway.

LeFevre, J., 1986. Aspects of biology of frontal systems, *Advanced Marine Biology*, 23:163-299.

Lewis, J.M., and J.C. Derber, 1985. The use of adjoint equations to solve a variational adjustment problem with advective constraints. *Tellus*, 37A(4):309-322.

Long, R.B., and W.C. Thacker, 1989, Data assimilation into a numerical equatorial ocean model. I. The model and the assimilation algorithm. *Dyn. Atmos. Oceans*, 13(3-4):379-412.

Krishen, K., 1973. Detection of Oil Spills Using a 13.3 GHz Radar Scatterometer. *Journal of Geophysical Research*, 78:1952-1964.

Luther, M.E., and J.J. O'Brien, 1985. A model of the seasonal circulation in the Arabian Sea forced by observed winds. *Progr. Oceanogr.*, 14:353-385.

Lyzenga, D.R., 1991. Interaction of Short Surface and Electromagnetic Waves With Ocean Fronts. *Journal of Geophysical Research*, 96:10765-10772.

Martinsen, E.A., and H. Engedahl, 1987. Implementation and testing of a lateral boundary scheme as an open boundary condition for a barotropic model. *Coastal Engineering*, 11:603-637.

McWilliams, J.C., W.B. Owens, and B.L. Hua, 1986. An objective analysis of the POLYMODE Local Dynamics Experiment. Part I: General formalism and statistical model selection. *J. Phys. Oceanogr.*, 16,(3):483-504.

Pettersson, L.H., O.M. Johannessen, and O. Frette, 1992. NORSMAP'89 - Norwegian Remote Sensing Spectrometry for Mapping and Monitoring of Algal Blooms and Pollution. *Proceedings from EISAC'89 Final Workshop*, Joint Research Centre, Ispar, Italy. In press at ESA/ESTEC.

Rienecker, M.M., and R.N. Miller, 1991. Ocean data assimilation using optimal interpolation with a quasi-geostrophic model. *J. Geophys. Res.*, 96(C8):15093-15103.

Rey, F., 1981. The development of the spring phytoplankton outburst at selected sites off the Norwegian Coast. *The Norwegian Coastal Current, Vol 2* (R. Saetre and M. Mork, editors), University of Bergen, Bergen Norway; pp. 649-680.

Talagrand, O., and P. Courtier, 1987. Variational assimilation of meteorological observations with the adjoint vorticity equation I: Theory. *Quart. J. Roy. Meteor. Soc.*, 113:1311-1328.

Thacker, W.C., and R.B. Long, 1988. Fitting dynamics to data. *J. Geophys. Res.*, 93(C2):1227-1240.

Woods, J., 1988. Mesoscale upwelling and primary production, *Towards a theory of biological-physical interactions in the World Ocean* (B.J. Rothschield, editor), D. Reidel, Dordrecht.

Wright, J.W., 1978. Detection of ocean waves by microwave radar: The modulation of short gravity-capillary waves. *Boundary Layer Meteorology*, 13:87-105.